Dissipation-Driven Transition of Particles from Dispersive to Flat Bands

Yutao Hu,[1, 2, 3] Chao Yang,[4, 1] and Yucheng Wang[1, 2, 3, *]

[1]*Shenzhen Institute for Quantum Science and Engineering,*
Southern University of Science and Technology, Shenzhen 518055, China
[2]*International Quantum Academy, Shenzhen 518048, China*
[3]*Guangdong Provincial Key Laboratory of Quantum Science and Engineering,*
Southern University of Science and Technology, Shenzhen 518055, China
[4]*Department of Physics, Southern University of Science and Technology, Shenzhen 518055, China*

Flat bands (FBs) play a crucial role in condensed matter physics, offering an ideal platform to study strong correlation effects and enabling applications in diffraction-free photonics and quantum devices. However, the study and application of FB properties are susceptible to interference from dispersive bands. Here, we explore the impact of bond dissipation on systems hosting both flat and dispersive bands by calculating the steady-state density matrix. We demonstrate that bond dissipation can drive particles from dispersive bands into FBs and establish the general conditions for this phenomenon to occur. Our results demonstrate that dissipation can facilitate FB preparation, property measurement, and utilization. This opens a new avenue for exploring FB physics in open quantum systems, with potential implications for strongly correlated physics.

Introduction. — Flat band (FB) systems have attracted widespread attention due to their quenched kinetic energy, leading to eigenmodes that are compactly localized in space. This makes the system highly sensitive to interactions, often giving rise to strongly correlated phenomena such as fractional Chern insulators [1–3], superconductors [3–7], Mott insulators [8, 9], and others. Even in non-interacting systems, FB systems can exhibit many interesting phenomena, such as the inverse Anderson transition [10–12], multifractal behavior and unconventional mobility edges [13–15], influenced by disorder or quasi-periodic potentials. FBs have also garnered significant experimental interest and have been realized in various systems, including solid-state systems [16, 17], cavity polaritons [18–20], photonic waveguides [21–23], superconducting wire networks [24, 25] and ultracold atoms in optical lattices [26–33]. In particular, recent advances in Moiré materials provide an intrinsic platform for studying the connection between FBs and quantum geometry, as well as the applications of FB systems [3–5, 34–38].

The formation of FBs typically arises from the destructive interference of wavefunctions in specific lattice structures [39–41], such as Lieb [42, 43], diamond [44, 45], stub [20, 46], Kagome [47, 48], or sawtooth [49, 50] lattices. This destructive interference leads to the formation of compact localized states (CLSs) in FBs. Given a single CLS, the whole CLS set can be generated through lattice translations. The CLS can be classified based on the minimum number U of unit cells they span [51, 52]. As shown in Fig. 1, the cross-stitch lattice and sawtooth lattice are examples corresponding to $U = 1$ and $U = 2$, respectively. Notably, it is rare to find a system where all the bands are flat. Typically, dispersive (non-flat) bands are still present, which may significantly influence both experimental measurements and practical applications of FB properties. Consequently, eliminating the influence of particles in the dispersive bands has both theoretical and

practical significance.

Dissipation occurs widely in various systems and profoundly impacts the properties of these systems. Although dissipation is generally considered harmful to quantum correlations, recent progress in experimental techniques for controlling various types of dissipation [53–76] has led to growing interest in using dissipation to control quantum states or phase transitions [56–69, 72–96]. In this Letter, we investigate a type of experimentally realizable bond dissipation applied to systems with FBs and show that it can drive the system into the FB, regardless of the initial state. This means that such dissipation can drive particles from the dispersive bands into the FB, thereby serving as a control mechanism to eliminate the influence of dispersive bands. This control effect is applicable to a variety of FB systems.

General discussion on the conditions for bond dissipation driving particles into the flatband. — The dynamical evolution of an open quantum system's density matrix under Markov approximation is governed by the Lindblad master equation [97, 98],

$$\frac{d\rho}{dt} = \mathcal{L}[\rho] = -i[H, \rho] + \Gamma \sum_j (O_j \rho O_j^\dagger - \frac{1}{2}\{O_j^\dagger O_j, \rho\}),$$

where $\mathcal{L}$ represents the Lindbladian, with the steady-state density matrix ρ_{ss} corresponding to its eigenstate with a zero eigenvalue, i.e., $\mathcal{L}[\rho_{ss}] = 0$. O_j represents the jump operator that acts on a pair of sites j and $j + q$, with a site-independent dissipation strength Γ, as defined by [77, 95, 99–103]:

$$O_j = (c_j^\dagger + ac_{j+q}^\dagger)(c_j - ac_{j+q}), \quad (1)$$

where $a = \pm 1$ and $q \geq 1$. This dissipation, termed bond dissipation, preserves the system's particle number but modifying the relative phase between pairs of sites separated by a distance q. It can drive particles into an

in-phase (out-of-phase) state, corresponding to $a = 1$ ($a = -1$). Such dissipation has been proposed to be realizable in cold atom systems [77, 95, 99, 100] and arrays of superconducting microwave resonators [101].

We now discuss the conditions for constructing dark states of bond dissipation described by Eq.(2) in FBs. For an eigenstate $|\Psi_n\rangle$, if it satisfies the condition that a set of dissipative operators O_j annihilate it, i.e.,

$$\forall j, \quad O_j|\Psi_n\rangle = 0, \qquad (2)$$

then $|\Psi_n\rangle$ is a dark state [99]. If such a dark state $|\Psi_n\rangle$ exists, the steady state of the system can be a pure state, given by $\rho_{ss} = |\Psi_n\rangle\langle\Psi_n|$. In a U-class FB system with L unit cells, there are $N = L/U$ CLSs. Any eigenstate on the FB can be constructed through the superposition of these N CLSs, i.e.,

$$|\Psi_n\rangle = \sum_{j=1}^{N} A_j|\phi_{\text{CLS}}^j\rangle, \qquad (3)$$

where A_j denotes the complex amplitude for the j-th CLS $|\phi_{\text{CLS}}^j\rangle$. We first treat a CLS as a whole, namely, $c_j^\dagger$ (c_j) in Eq. (1) represents the creation (annihilation) operator of the j-th CLS. From Eqs. (1, 2, 3), it is straightforward to see that when A_j, $|\phi_{\text{CLS}}^j\rangle$, and q satisfy the following three conditions:

$$A_j = A_{j+\kappa}, \quad |\phi_{\text{CLS}}^{j+\kappa}\rangle = a|\phi_{\text{CLS}}^j\rangle, \quad \text{and} \quad q = \kappa, \qquad (4)$$

where $\kappa \geq 1$ is an integer, the FB state in Eq.(3) will become a dark state that satisfies Eq.(2). In FB systems, lattice translations of a single CLS generate multiple CLSs that are spatially distinct and phase-uncorrelated, allowing independent manipulation through bond dissipation to satisfy the dark state's phase relationship requirements. Moreover, any linear combination of these CLSs constitutes an eigenstate in the FB, allowing the coefficients A_j to be freely tuned to satisfy dark state formation conditions. Thus, the first two conditions in Eq.(4) can be satisfied for any sign of a. In Eqs. (3, 4), j indexes the CLS, each spanning U unit cells in a U-class FB system. For a multi-chain system, each unit cell contains sites per chain. The third condition above, where q spans κ CLSs (i.e., $q = \kappa$), implies that on each chain this corresponds to κU unit cells, while requiring the bond dissipation to maintain identical form across different chains. That is, the conditions for CLSs on a FB to form a dark state under bond dissipation are:

$$q = \kappa U, \quad \text{and} \quad O_j^1 = O_j^\alpha (\alpha > 1), \qquad (5)$$

where O_j^α denotes bond dissipation on the α-th chain, which has the same form as the bond dissipation on the first chain O_j^1. This requirement arises because the amplitude distribution and phase relationships among lattice sites within a single CLS are fixed. The bond dissipation on one chain determines the phase relationships
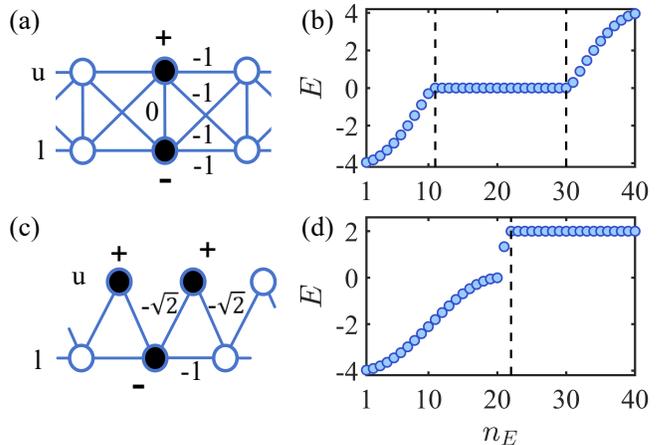

Figure 1: (a) and (c): Circles denote lattice sites, and filled circles indicate the distribution of a CLS. (a) Cross-stitch lattice with a $U = 1$ CLS configuration, with the corresponding energy spectrum shown in (b). We set the inter-cell hopping to -1 and the intra-cell hopping to 0. (c) Sawtooth lattice with a $U = 2$ CLS configuration, with the corresponding energy spectrum shown in (d). The intra-cell hopping is set to $-\sqrt{2}$, while the inter-cell hoppings are $-\sqrt{2}$ between the upper and lower chains and -1 between the lower chain sites. Throughout this work, we set the onsite energies to 0 and use open boundary conditions.

between its sites, which in turn fixes those on the other chains to satisfy the CLS pattern. As a result, the form of bond dissipation applied to the other chains is also constrained. We need to clarify two points: 1. Eq.(5) does not require the dissipation strength Γ to be the same across all chains. Even applying bond dissipation on only one chain (with $\Gamma = 0$ on the others) can still drive the steady state into the FB. In other words, the phase relationship between lattice sites is determined through bond dissipation on a single chain, and the occupation on other chains is subsequently fixed accordingly, while also satisfying the occupation ratio required by the CLS. 2. The requirement on q in Eq. (5) can be relaxed for some specific CLS distributions (see Supplemental Material [104]).

When the bond dissipation follows the form prescribed in Eq. (5), the system's steady state will always populate the FB, regardless of the initial state. Below, we will illustrate this point using the cross-stitch model and the sawtooth model as examples [Fig. 1]. Both models consist of upper and lower chains, with each unit cell containing two lattice sites. The wave function is written as $|\Psi\rangle = (\ldots, \psi_{j-1}, \psi_j, \ldots)$, where each ψ_j is a two-component vector representing the amplitudes on the upper and lower sites of the j-th unit cell. Using the eigenvalue equation $H\Psi = E\Psi$, we obtain:

$$H_{-1}\psi_{j-1} + H_0\psi_j + H_1\psi_{j+1} = E\psi_j, \qquad (6)$$

where the 2×2 matrices $H_1 = H_{-1}^\dagger$ describe the hopping between the lattice sites of neighboring unit cells, and H_0
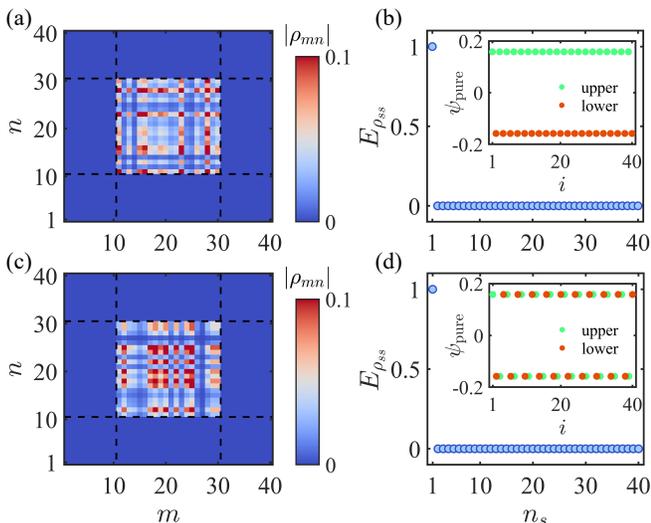
Figure 2: Steady-state properties of the cross-stitch model after introducing bond dissipation with $q = 1$ and $O_j^u = O_j^l$. The absolute values of the steady state's density matrix elements for (a) $a = 1$ and (c) $a = -1$ in the eigenbasis of H. The dashed lines separate the FB region in the middle from the dispersive band regions on the sides [see Fig. 1(b)]. Eigenvalue distribution of the steady-state density matrix for (b) $a = 1$ and (d) $a = -1$, both having only one non-zero eigenvalue. The eigenstate corresponding to the non-zero eigenvalue is shown in real space in the respective inset. Here, we consider 20 unit cells. We set the dissipation strength $\Gamma = 1$ on each chain. The results remain unchanged even if the strengths on the two chains are unequal, or if $\Gamma = 0$ on one of them.

describes the on-site potentials and the hopping between lattice sites within the same unit cell.

Cross-stitch model.— We begin by examining the impact of bond dissipation on the cross-stitch model [Fig. 1(a)]. In the absence of on-site potentials, the system features exactly one FB and one dispersive band [51]. We set the inter-cell hopping strength to t_1, which applies both along the same chain and between the upper and lower chains across unit cells, and set the intra-cell hopping strength to t_0 for hopping between the upper and lower chains within the same unit cell. Consequently, H_0 and H_1 in Eq.(6) are expressed as

$$H_0 = -t_0 \begin{pmatrix} 0 & 1 \\ 1 & 0 \end{pmatrix}, \qquad H_1 = -t_1 \begin{pmatrix} 1 & 1 \\ 1 & 1 \end{pmatrix}. \qquad (7)$$

The position of the FB is determined by the intra-cell hopping strength t_0 and is given by $E_{FB} = t_0$. Without loss of generality, we set $t_1 = 1$ and $t_0 = 0$ [Fig. 1(a)], such that a FB exists at $E_{FB} = 0$ [Fig. 1(b)]. This FB supports a series of CLSs with the wave function $|\phi_{\text{CLS}}\rangle = (1, -1)^T$ [Fig. 1(a)], which is strictly localized within a single unit cell.

As specified in Eq. (5), the implemented jump operators satisfy two requirements: (1) For the cross-stitch lattice, which belongs to the $U = 1$ class model, the condition reduces to $q \geq 1$; (2) The bond dissipation operators are identical for the upper and lower chains, i.e., $O_j^u = O_j^l$, where O_j^u (or O_j^l) represents the jump operator acting on the upper (or lower) chain. In the Supplemental Material [104], we discuss the physical effects arising from $O_j^u \neq O_j^l$. Our results are independent of the dissipation strength Γ, which can vary across chains, even with $\Gamma = 0$ on one chain. Without loss of generality, we set the dissipation strength on each chain to 1. We first fix $q = 1$ and $a = 1$. We proceed to examine the properties of the stationary solution ρ_{ss} within the eigenbasis of the Hamiltonian H, expressed as $\rho_{mn} = \langle \Psi_m | \rho_{ss} | \Psi_n \rangle$, where $|\Psi_m\rangle$ and $|\Psi_n\rangle$ represent the eigenstates of H. Fig. 2(a) illustrates that the system's steady state occupies the FB region, which is independent of the initial state. Therefore, this bond dissipation can drive particles from the dispersive band into the FB. Diagonalizing the steady-state density matrix ρ_{ss} reveals its eigenvalues, as shown in Fig. 2(b), where only one non-zero eigenvalue is present, indicating that ρ_{ss} corresponds to a pure state. The inset in Fig. 2(b) displays the real-space wave function distribution of this pure state, where $i = 2j - 1$ (or $2j$) corresponds to the upper (or lower) chain of the j-th unit cell, showing the out-of-phase on the upper and lower chains within the same unit cell (consistent with the distribution of the CLS in the FB, $|\phi_{\text{CLS}}\rangle = (1, -1)^T$) while maintaining the in-phase across different unit cells on the same chain, a behavior resulting from setting $a = 1$ in the bond dissipation. Therefore, this pure state is constructed from an equal-weight superposition of CLSs of the cross-stitch model: $|\Psi_{\text{pure}}\rangle = \sum_j^L A |\phi_{\text{CLS}}^j\rangle$. When $a = -1$, the steady state of the system remains in the FB region [Fig. 2(c)], and ρ_{ss} still corresponds to a pure state [Fig. 2(d)]. However, this pure state exhibits alternating phases between neighboring unit cells on the same chain, as shown in the inset of Fig. 2(d), which arises because the bond dissipation with $a = -1$ selects the out-of-phase. In this case, the pure state can be expressed in terms of CLSs as: $|\Psi_{\text{pure}}\rangle = \sum_j^L (-1)^j A |\phi_{\text{CLS}}^j\rangle$.

When $q > 1$, it is numerically straightforward to show that the steady state of the system still occupies the FB region, but the number of steady states will increase. Fig. 3(a) and Fig. 3(b) respectively display the real parts of the eigenvalues, $\text{Re}(E_{\mathcal{L}})$, of the Liouvillian superoperator $\mathcal{L}$ for $q = 1$ and $q = 2$ with fixed $a = 1$. Here $\mathcal{L}$ is represented as a $(2L)^2 \times (2L)^2$ matrix, where L denotes the number of unit cells. One can see that for $q = 1$ and $q = 2$, there are numerically one and four values, respectively, for which $\text{Re}(E_{\mathcal{L}}) \to 0$, indicating that the system has one and four steady states. To understand why four steady states appear when $q = 2$, we regroup the q sites on each chain into a single unit, labeled as d, as shown in Fig. 3(c). The bond dissipation in Eq.(1) with $q = 2$ affects next-nearest-neighbor sites, meaning that sites 1 and 2 in different units are independently influenced. This leads to the formation of two
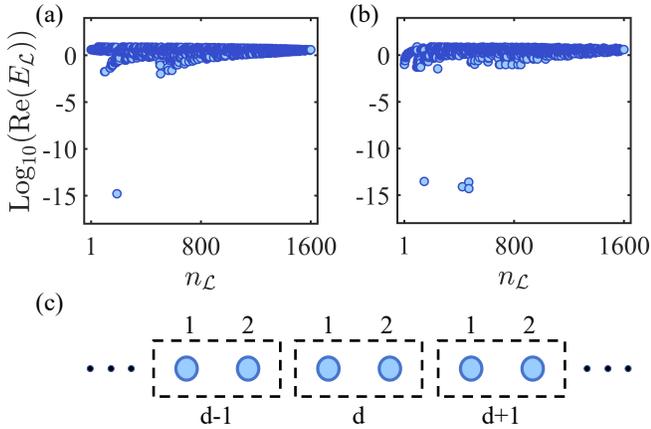
Figure 3: The real parts of the eigenvalues of the Liouvillian superoperator for (a) $q = 1$ and (b) $q = 2$. Here, we fix $a = 1$ and $L = 20$. (c) To explain the emergence of the fourfold steady state for $q = 2$, we redefine each pair of lattice sites on a single chain of the cross-stitch model as a new unit.

Figure 4: The steady-state properties of the sawtooth model under bond dissipation with $q = 2$ and $O_j^u = O_j^l$. The steady-state density matrix elements for (a) $a = 1$ and (b) $a = -1$ in the eigenbasis of H. The dashed lines mark the boundary between the FB and dispersive band regions [see Fig. 1(d)]. Eigenvalue distribution of the steady-state density matrix for (c) $a = 1$ and (d) $a = -1$, both featuring a single nonzero eigenvalue. The real-space distribution of the corresponding eigenstate is shown in the insets. Here, we fix $L = 20$.

dark states that satisfy Eq.(2): $|\Psi_{\text{dark}}^{(1)}\rangle = \sum_d A|\phi_{\text{CLS}}^{2d-1}\rangle$ and $|\Psi_{\text{dark}}^{(2)}\rangle = \sum_d B|\phi_{\text{CLS}}^{2d}\rangle$, both of which lie on the FB. These two dark states span a 2D steady-state subspace, with the corresponding density matrix having a dimension of 4. The steady-state density matrix is given by: $\rho_{ss} = \sum_{i,j=1}^2 C_{ij}|\Psi_{\text{dark}}^{(i)}\rangle\langle\Psi_{\text{dark}}^{(j)}|$, where the coefficients C_{ij} form a positive semi-definite, Hermitian and unit trace matrix. The method of utilizing such bond dissipation with $q > 1$ to prepare multiple steady states can also be easily extended to systems without FBs, potentially leading to important applications.

Sawtooth model.— We next take the sawtooth model as an example to study the effect of bond dissipation on $U = 2$-type FB systems. When the onsite energies are the same (set to 0 here), and the ratio of the diagonal hopping between the upper and lower chains to the baseline hopping within the lower chain is $\sqrt{2}$ [see Fig. 1(c)], i.e., the system's Hamiltonian is given by [51, 52]

$$H_0 = -\begin{pmatrix} 0 & \sqrt{2} \\ \sqrt{2} & 0 \end{pmatrix}, \qquad H_1 = -\begin{pmatrix} 0 & \sqrt{2} \\ 0 & 1 \end{pmatrix}, \qquad (8)$$

this configuration results in a FB, as shown in Fig. 1(d). The FB contains a series of CLSs, each of which occupies two unit cells, given by $|\phi_{\text{CLS}}\rangle = ((1,0)^T, (1,-\sqrt{2})^T)$ [Fig. 1(c)].

Since the sawtooth model belongs to the $U = 2$ class, according to Eq. (5), the form of the applied bond dissipation satisfies $q = 2\kappa$. Additionally, another requirement is the same as the second condition for the bond dissipation applied to the cross-stitch model: $O_j^u = O_j^l$. We first fix $q = 2$ (i.e., $\kappa = 1$). Figures 4(a) and 4(b) display the steady-state density matrix in the Hamiltonian's eigenbasis for $a = 1$ and $a = -1$, respectively, demonstrating that the system's steady state always occupies
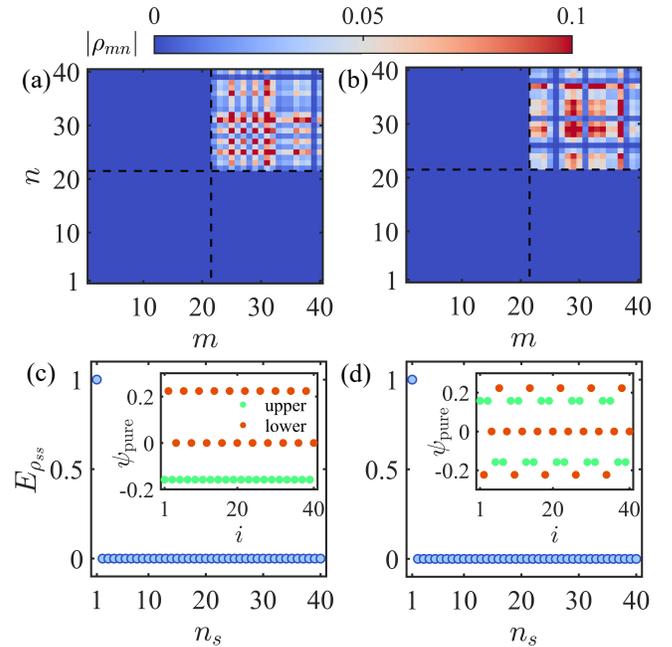
the FB region. Moreover, in both cases, the steady-state density matrix ρ_{ss} exhibits only one nonzero eigenvalue [see Figs. 4(c) and 4(d)], indicating that the final steady state is a pure state. For $a = 1$, the pure state exhibits an in-phase distribution between next-nearest-neighbor lattice sites on the same chain (see inset in Fig. 4(c)), while for $a = -1$, it shows out-of-phase distribution (see inset in Fig. 4(d)). Combining with the form of the CLS in this model, these two pure states can be respectively expressed in terms of CLS as: $|\Psi_{\text{pure}}\rangle = \sum_j^N A|\phi_{\text{CLS}}^j\rangle$ and $|\Psi_{\text{pure}}\rangle = \sum_j^N (-1)^j A|\phi_{\text{CLS}}^j\rangle$, where $N = L/U$ represents the total number of CLS.

Conclusion and Discussion.— We have demonstrated that bond dissipation satisfying the form of Eq. (5) can drive particles from dispersive bands into FBs. Upon reaching the steady state, the dissipation can be removed, after which the density matrix evolves in time as $\rho(t) = \sum_{nm} e^{i(E_n - E_m)t}\rho_{nm}|\Psi_n\rangle\langle\Psi_m|$, where E_n and E_m are the eigenvalues corresponding to the eigenstates $|\Psi_n\rangle$ and $|\Psi_m\rangle$ of the Hamiltonian H, respectively. Clearly, the diagonal elements $\rho_{nn}(t) = \rho_{nn}$ remain constant over time. This indicates that the particles occupy only the FB regions, just as in the steady state. Thus, by temporarily applying dissipation and then removing it, the

Hamiltonian's parameters and spectral structure stay unchanged, but particles originally in dispersive bands are driven into the FBs.

Our results can be experimentally investigated using cold atoms in optical lattices. Numerous models featuring FBs have already been realized in cold-atom systems [26–33], including the cross-stitch lattice [28] and sawtooth lattice [27] discussed in this work. Furthermore, the experimental scheme for implementing bond dissipation [Eq.(1)] was originally proposed using cold-atom platforms [77, 99, 100]. The initial approach involved introducing a driving laser to achieve the $q = 1$ case by adjusting the relationship between the wavelength of the driving laser and the optical lattice [77, 99, 100]. Recent work has demonstrated that by modulating the polarization of the driving laser to achieve coupling between specific internal states, cases such as $q = 2$ or even $q > 2$ can be realized [95]. While we have primarily used the cross-stitch lattice and sawtooth lattice as examples in this work, our results can be generally applied to other quasi-one-dimensional FB systems. In future research, we will extend our results to interacting systems and two-dimensional FB systems.

Using dissipation eliminates the influence of particles in dispersive bands, which facilitates the study of phenomena related to FB physics and holds potential applications in strongly correlated systems, including theoretical studies, experimental investigations, and material preparation. Our work opens a new avenue for leveraging dissipation to drive particles into FBs, offering fresh insights into the study of FBs in open systems. Although experimental realization of this studied bond dissipation in materials remains challenging, leveraging the unique properties of FBs may enable identification of feasible dissipative configurations in material systems that can generate analogous physical effects.

————————————

* Corresponding author: wangyc3@sustech.edu.cn

[1] Y.-F. Wang, Z.-C. Gu, C.-D. Gong, and D. N. Sheng, Fractional Quantum Hall Effect of Hard-Core Bosons in Topological Flat Bands Phys. Rev. Lett. **107**, 146803 (2011); W.-W. Luo, A.-L. He, Y. Zhou, Y.-F. Wang, and C.-D. Gong, Quantum phase transitions in a $\nu = 1/2$ bosonic fractional Chern insulator, Phys. Rev. B **102**, 155120 (2020).

[2] R. Roy and S. Sondhi, Fractional quantum hall effect without Landau levels, Physics **4**, 46 (2011).

[3] T. Liu, X.-B. Qiang, H.-Z. Lu, and X. C. Xie, Quantum geometry in condensed matter, National Science Review, 12, nwae334 (2025).

[4] Y. Cao, V. Fatemi, S. Fang, K. Watanabe, T. Taniguchi, E. Kaxiras, and P. Jarillo-Herrero, Unconventional superconductivity in magic-angle graphene superlattices, Nature **556**, 43 (2018).

[5] M. Yankowitz, S. Chen, H. Polshyn, Y. Zhang, K. Watanabe, T. Taniguchi, D. Graf, A. F. Young, and C. R. Dean, Tuning superconductivity in twisted bilayer graphene, Science **363**, 1059 (2019).

[6] V. I. Iglovikov, F. Hébert, B. Grémaud, G. G. Batrouni, and R. T. Scalettar, Superconducting transitions in flat-band systems, Phys. Rev. B **90**, 094506 (2014).

[7] N. B. Kopnin, T. T. Heikkilä, and G. E. Volovik, High-temperature surface superconductivity in topological flat-band systems, Phys. Rev. B **83**, 220503 (2011).

[8] S. Guo, et al, Discovery of a Single-Band Mott Insulator in a van der Waals Flat-Band Compound, Phys. Rev. X **13**, 041049 (2023).

[9] H. C. Po, L. Zou, A. Vishwanath, and T. Senthil, Origin of Mott Insulating Behavior and Superconductivity in Twisted Bilayer Graphene, Phys. Rev. X **8**, 031089 (2018).

[10] M. Goda, S. Nishino, and H. Matsuda, Inverse Anderson Transition Caused by Flatbands, Phys. Rev. Lett. **96**, 126401 (2006).

[11] S. Nishino, H. Matsuda, and M. Goda, Flat-Band Localization in Weakly Disordered System, J. Phys. Soc. Jpn. **76**, 024709 (2007).

[12] W. Zhang, H. Wang, H. Sun, and X. Zhang, Non-Abelian Inverse Anderson Transitions, Phys. Rev. Lett. **130**, 206401 (2023).

[13] J. D. Bodyfelt, D. Leykam, C. Danieli, X. Yu, and S. Flach, Flatbands under Correlated Perturbations, Phys. Rev. Lett. **113**, 236403 (2014).

[14] Y. Wang, L. Zhang, Y. Wan, Y. He, and Y. Wang, Two-dimensional vertex-decorated Lieb lattice with exact mobility edges and robust flat bands, Phys. Rev. B 107, L140201 (2023).

[15] S.-Z. Li, Y.-C. Zhang, Y. Wang, S. Zhang, S.-L. Zhu, and Z. Li, Multifractal-enriched mobility edges and emergent quantum phases in one-dimensional exactly solvable lattice models, arXiv:2501.07866.

[16] R. Drost, T. Ojanen, A. Harju, and P. Liljeroth, Topological states in engineered atomic lattices, Nat. Phys. **13**, 668 (2017).

[17] M. R. Slot, T. S. Gardenier, P. H. Jacobse, G. C. P. van Miert, S. N. Kempkes, S. J. M. Zevenhuizen, C. M. Smith, D. Vanmaekelbergh, and I. Swart, Experimental realization and characterization of an electronic Lieb lattice, Nat. Phys. **13**, 672 (2017).

[18] V. Goblot, B. Rauer, F. Vicentini, A. Le Boité, E. Galopin, A. Lemaître, L. Le Gratiet, A. Harouri, I. Sagnes, S. Ravets, C. Ciuti, A. Amo, and J. Bloch, Nonlinear Polariton Fluids in a Flatband Reveal Discrete Gap Solitons, Phys. Rev. Lett. **123**, 113901 (2019).

[19] T. H. Harder, O. A. Egorov, J. Beierlein, P. Gagel, J. Michl, M. Emmerling, C. Schneider, U. Peschel, S. Höfling, and S. Klembt, Exciton-polaritons in flatland: Controlling flatband properties in a Lieb lattice, Phys. Rev. B 102, 121302(R) (2020).

[20] F. Baboux, L. Ge, T. Jacqmin, M. Biondi, A. Lemaître, L. Le Gratiet, I. Sagnes, S. Schmidt, H. E. Türeci, A. Amo, J. Bloch, Bosonic Condensation and Disorder-Induced Localization in a Flat Band, Phys. Rev. Lett. **116**, 066402 (2016).

[21] R. A. Vicencio, C. Cantillano, L. Morales-Inostroza, B. Real, C. Mejía-Cortés, S. Weimann, A. Szameit, and M. I. Molina, Observation of Localized States in Lieb Photonic Lattices, Phys. Rev. Lett. **114**, 245503 (2015).

[22] S. Mukherjee, A. Spracklen, D. Choudhury, N. Goldman, P. Öhberg, E. Andersson, and R. R. Thomson, Observation of a Localized Flat-Band State in a Photonic Lieb Lattice, Phys. Rev. Lett. **114**, 245504 (2015).

[23] S. Mukherjee, M. Di Liberto, P. Öhberg, R. R. Thomson, and N. Goldman, Experimental Observation of Aharonov-Bohm Cages in Photonic Lattices, Phys. Rev. Lett. **121**, 075502 (2018).

[24] J. Vidal, R. Mosseri, and B. Douçot, Aharonov-Bohm cages in two-dimensional structures, Phys. Rev. Lett. **81**, 5888 (1998).

[25] C. C. Abilio, P. Butaud, Th. Fournier, B. Pannetier, J. Vidal, S. Tedesco, and B. Dalzotto, Magnetic field induced localization in a two-dimensional superconducting wire network, Phys. Rev. Lett. **83**, 5102 (1999).

[26] G.-B. Jo, J. Guzman, C. K. Thomas, P. Hosur, A. Vishwanath, and D. M. Stamper-Kurn, Ultracold Atoms in a Tunable Optical Kagome Lattice, Phys. Rev. Lett. **108**, 045305 (2012).

[27] C. Zeng, Y.-R. Shi, Y.-Y. Mao, F.-F. Wu, Y.-J. Xie, T. Yuan, W. Zhang, H.-N. Dai, Y.-A. Chen, and J.-W. Pan, Transition from Flat-Band Localization to Anderson Localization in a One-Dimensional Tasaki Lattice, Phys. Rev. Lett. **132**, 063401 (2024).

[28] Y. He, R. Mao, H. Cai, J.-X. Zhang, Y. Li, L. Yuan, S.-Y. Zhu, and D.-W. Wang, Flat-Band Localization in Creutz Superradiance Lattices, Phys. Rev. Lett. **126**, 103601 (2021).

[29] T.-H. Leung, M. N. Schwarz, S.-W. Chang, C. D. Brown, G. Unnikrishnan, and D. Stamper-Kurn, Interaction-Enhanced Group Velocity of Bosons in the Flat Band of an Optical Kagome Lattice, Phys. Rev. Lett. **125**, 133001 (2020).

[30] S. Taie, H. Ozawa, T. Ichinose, T. Nishio, S. Nakajima, and Y. Takahashi, Coherent driving and freezing of bosonic matter wave in an optical Lieb lattice, Sci. Adv. **1**, e1500854 (2015).

[31] J. Jünemann, A. Piga, S.-J. Ran, M. Lewenstein, M. Rizzi, and A. Bermudez, Exploring Interacting Topological Insulators with Ultracold Atoms: The Synthetic Creutz-Hubbard Model, Phys. Rev. X **7**, 031057 (2017).

[32] T. Chen, C. Huang, I. Velkovsky, T. Ozawa, H. Price, J. P. Covey, and B. Gadway, Interaction-driven breakdown of Aharonov-Bohm caging in flat-band Rydberg lattices, Nat. Phys. **21**, 221 (2025).

[33] H. Li, Q. Liang, Z. Dong, H. Wang, W. Yi, J.-S. Pan, and B. Yan, Engineering topological chiral transport in a flat-band lattice of ultracold atoms, arXiv:2401.03611.

[34] R. Bistritzer and A. H. MacDonald, Moiré bands in twisted double-layer graphene, PNAS **108**, 12233 (2011).

[35] Y. Cao, V. Fatemi, A. Demir, S. Fang, S. L. Tomarken, J. Y. Luo, J. D. Sanchez-Yamagishi, K. Watanabe, T. Taniguchi, E. Kaxiras, R. C. Ashoori, and P. Jarillo-Herrero, Correlated insulator behaviour at half-filling in magic-angle graphene superlattices, Nature **556**, 80 (2018).

[36] X. Lu, P. Stepanov, W. Yang, M. Xie, M. A. Aamir, I. Das, C. Urgell, K. Watanabe, T. Taniguchi, G. Zhang, A. Bachtold, A. H. MacDonald, and D. K. Efetov, Superconductors, orbital magnets and correlated states in magic-angle bilayer graphene, Nature 574, 653 (2019).

[37] A. L. Sharpe, E. J. Fox, A. W. Barnard, J. Finney, K. Watanabe, T. Taniguchi, M. A. Kastner, and D. Goldhaber-Gordon, Emergent ferromagnetism near three-quarters filling in twisted bilayer graphene, Science **365**, 605 (2019).

[38] Y. Xie, B. Lian, B. Jäck, X. Liu, C.-L. Chiu, K. Watanabe, T. Taniguchi, B. A. Bernevig, and A. Yazdani, Spectroscopic signatures of many-body correlations in magic-angle twisted bilayer graphene, Nature **572**, 101 (2019).

[39] D. Călugăru, A. Chew, L. Elcoro, Y. Xu, N. Regnault, Z.-D. Song, and B. A. Bernevig, General construction and topological classification of crystalline flat bands, Nat. Phys. **18**, 185 (2022).

[40] L. Morales-Inostroza and R. A. Vicencio, Simple method to construct flat-band lattices, Phys. Rev. A **94**, 043831 (2016).

[41] T.-F. J. Poon, Y. Wan, Y. Wang, and X.-J. Liu, Anomalous universal quantum transport in 2D asymptotic quasiperiodic system, arXiv:2312.04349.

[42] E. H. Lieb, Two Theorems on the Hubbard Model, Phys. Rev. Lett. **62**, 1201 (1989).

[43] A. Julku, S. Peotta, T. I. Vanhala, D.-H. Kim, and P. Törmä, Geometric Origin of Superfluidity in the Lieb-Lattice Flat Band, Phys. Rev. Lett. **117**, 045303 (2016).

[44] S. Mukherjee and R. R. Thomson, Observation of localized flat-band modes in a quasi-one-dimensional photonic rhombic lattice, Opt. Lett. **40**, 5443 (2015).

[45] G. Cáceres-Aravena, D. Guzmán-Silva, I. Salinas, and R. A. Vicencio, Controlled Transport Based on Multiorbital Aharonov-Bohm Photonic Caging Phys. Rev. Lett. **128**, 256602 (2022).

[46] M. Hyrkäs, V. Apaja, and M. Manninen, Many-particle dynamics of bosons and fermions in quasi-one-dimensional flat-band lattices, Phys. Rev. A **87**, 023614 (2013).

[47] S. D. Huber and E. Altman, Bose condensation in flat bands, Phys. Rev. B **82**, 184502 (2010).

[48] S. A. Parameswaran, I. Kimchi, A. M. Turner, D. M. Stamper-Kurn, and A. Vishwanath, Wannier Permanent Wave Functions for Featureless Bosonic Mott Insulators on the 1/3-Filled Kagome Lattice, Phys. Rev. Lett. **110**, 125301 (2013).

[49] T. Zhang and G.-B. Jo, One-dimensional sawtooth and zigzag lattices for ultracold atoms, Sci. Rep. **5**, 16044 (2015).

[50] S. Weimann, L. Morales-Inostroza, B. Real, C. Cantillano, A. Szameit, and R.A. Vicencio, Transport in Sawtooth photonic lattices, Opt. Lett. **41**, 2414 (2016).

[51] S. Flach, D. Leykam, J. D. Bodyfelt, P. Matthies, and A. S. Desyatnikov, Detangling flat bands into Fano lattices, Europhys. Lett. **105**, 30001 (2014).

[52] W. Maimaiti, A. Andreanov, H. C. Park, O. Gendelman, and S. Flach, Compact localized states and flat-band generators in one dimension, Phys. Rev. B **95**, 115135 (2017).

[53] H. Ritsch, P. Domokos, F. Brennecke, and T. Esslinger,

Cold atoms in cavity-generated dynamical optical potentials, Rev. Mod. Phys. **85**, 553 (2013).

[54] J. Barreiro, M. Müller, P. Schindler, D. Nigg, T. Monz, M. Chwalla, M. Hennrich, C. Roos, P. Zoller, and R. Blatt, An open-system quantum simulator with trapped ions, Nature **470**, 486 (2011).

[55] H. Weimer, M. Müller, I. Lesanovsky, P. Zoller, and H. P. Büchler, A Rydberg quantum simulator, Nat. Phys. **6**, 382 (2010).

[56] M. Müller, S. Diehl, G. Pupillo, and P. Zoller, Engineered open systems and quantum simulations with atoms and ions, Advances in Atomic, Molecular, and Optical Physics **61**, 1 (2012).

[57] H. Krauter, C. A. Muschik, K. Jensen, W. Wasilewski, J. M. Petersen, J. I. Cirac, and E. S. Polzik, Entanglement Generated by Dissipation and Steady State Entanglement of Two Macroscopic Objects, Phys. Rev. Lett. **107**, 080503 (2011).

[58] D. Kienzler, H.-Y. Lo, B. Keitch, L. de Clercq, F. Leupold, F. Lindenfelser, M. Marinelli, V. Negnevitsky, and J. P. Home, Quantum harmonic oscillator state synthesis by reservoir engineering, Science **347**, 53 (2015).

[59] Z. Leghtas, S. Touzard, I. M. Pop, A. Kou, B. Vlastakis, A. Petrenko, K. M. Sliwa, A. Narla, S. Shankar, M. J. Hatridge, M. Reagor, L. Frunzio, R. J. Schoelkopf, M. Mirrahimi, and M. H. Devoret, Confining the state of light to a quantum manifold by engineered two-photon loss, Science **347**, 853 (2015).

[60] P. M. Harrington, E. J. Mueller, and K. W. Murch, Engineered dissipation for quantum information science, Nat. Rev. Phys. **4**, 660 (2022).

[61] N. Syassen, D. M. Bauer, M. Lettner, T. Volz, D. Dietze, J. J. Garcia-Ripoll, J. I. Cirac, G. Rempe, and S. Dürr, Strong dissipation inhibits losses and induces correlations in cold molecular gases, Science **320**, 1329 (2008).

[62] V. A. Brazhnyi, V. V. Konotop, V. M. Pérez-García, and H. Ott, Dissipation-induced coherent structures in Bose-Einstein condensates, Phys. Rev. Lett. **102**, 144101 (2009).

[63] T. Tomita, S. Nakajima, I. Danshita, Y. Takasu, and Y. Takahashi, Observation of the Mott insulator to superfluid crossover of a driven-dissipative Bose-Hubbard system, Science Advances **3**, e1701513 (2017).

[64] N. Dogra, M. Landini, K. Kroeger, L. Hruby, T. Donner, and T. Esslinger, Dissipation-induced structural instability and chiral dynamics in a quantum gas, Science **366**, 1496 (2019).

[65] R. Bouganne, M. Bosch Aguilera, A. Ghermaoui, J. Beugnon, and F. Gerbier, Anomalous decay of coherence in a dissipative many-body system, Nat. Phys. **16**, 21 (2020).

[66] D. Dreon, A. Baumgärtner, X. Li, S. Hertlein, T. Esslinger, and T. Donner, Self-oscillating pump in a topological dissipative atom-cavity system, Nature **608**, 494 (2022).

[67] S. Viciani, M. Lima, M. Bellini, and F. Caruso, Observation of Noise-Assisted Transport in an All-Optical Cavity-Based Network, Phys. Rev. Lett. **115**, 083601 (2015).

[68] C. Maier, T. Brydges, P. Jurcevic, N. Trautmann, C. Hempel, B. P. Lanyon, P. Hauke, R. Blatt, and C. F. Roos, Environment-Assisted Quantum Transport in a 10-Qubit Network, Phys. Rev. Lett. **122**, 050501 (2019).

[69] R. Labouvie, B. Santra, S. Heun, and H. Ott, Bistability in a driven-dissipative superfluid, Phys. Rev. Lett. **116**, 235302 (2016).

[70] M. Lebrat, S. Häusler, P. Fabritius, D. Husmann, L. Corman, and T. Esslinger, Quantized conductance through a spin-selective atomic point contact, Phys. Rev. Lett. 123, 193605 (2019).

[71] M.-Z. Huang, J. Mohan, A.-M. Visuri, P. Fabritius, M. Talebi, S. Wili, S. Uchino, T. Giamarchi, and T. Esslinger, Superfluid signatures in a dissipative quantum point contact, Phys. Rev. Lett. **130**, 200404 (2023).

[72] R. El-Ganainy, K.G. Makris, M. Khajavikhan, Z.H. Musslimani, S. Rotter, and D.N. Christodoulides, Non-Hermitian physics and PT symmetry, Nat. Phys. **14**, 11(2018).

[73] Ş. K. Özdemir, S. Rotter, F. Nori, and L. Yang, Parity-time symmetry and exceptional points in photonics, Nat. Mater. **18**, 783 (2019).

[74] Y. Sun, T. Shi, Z. Liu, Z. Zhang, L. Xiao, S. Jia, and Y. Hu, Fractional Quantum Zeno Effect Emerging from Non-Hermitian Physics, Phys. Rev. X **13**, 031009 (2023).

[75] L. Xiao, T. Deng, K. Wang, Z. Wang, W. Yi, and P. Xue, Observation of Non-Bloch Parity-Time Symmetry and Exceptional Points, Phys. Rev. Lett. **126**, 230402 (2021); P. Xue, Q. Lin, K. Wang, L. Xiao, S. Longhi, and W. Yi, Self acceleration from spectral geometry in dissipative quantum-walk dynamics, Nat. Commun. **15**, 4381 (2024); L. Xiao, W.-T. Xue, F. Song, Y.-M. Hu, W. Yi, Z. Wang, and P. Xue, Observation of Non-Hermitian Edge Burst in Quantum Dynamics, Phys. Rev. Lett. **133**, 070801 (2024).

[76] J. Zhu, Y.-L. Mao, H. Chen, K.-X. Yang, L. Li, B. Yang, Z.-D. Li, and J. Fan, Observation of Non-Hermitian Edge Burst Effect in One-Dimensional Photonic Quantum Walk, Phys. Rev. Lett. **132**, 203801 (2024).

[77] S. Diehl, A. Micheli, A. Kantian, B. Kraus, H. P. Büchler, and P. Zoller, Quantum states and phases in driven open quantum systems with cold atoms, Nat. Phys. **4**, 878 (2008); S. Diehl, A. Tomadin, A. Micheli, R. Fazio, and P. Zoller, Dynamical phase transitions and instabilities in open atomic many-body systems, Phys. Rev. Lett. **105**, 015702 (2010); S. Diehl, E. Rico, M. A. Baranov, and P. Zoller, Topology by dissipation in atomic quantum wires, Nat. Phys. **7**, 971 (2011).

[78] F. Carollo, A. Lasanta, and I. Lesanovsky, Exponentially Accelerated Approach to Stationarity in Markovian Open Quantum Systems through the Mpemba Effect, Phys. Rev. Lett. **127**, 060401 (2021); A. K. Chatterjee, S. Takada, and H. Hayakawa, Quantum Mpemba Effect in a Quantum Dot with Reservoirs, Phys. Rev. Lett. **131**, 080402 (2023).

[79] H.-P. Breuer, E.-M. Laine, J. Piilo, and B. Vacchini, Colloquium: Non-Markovian dynamics in open quantum systems, Rev. Mod. Phys. **88**, 021002 (2016); I. de Vega and D. Alonso, Dynamics of non-Markovian open quantum systems, Rev. Mod. Phys. **89**, 015001 (2017).

[80] E. J. Bergholtz, J. C. Budich, and F. K. Kunst, Exceptional topology of non-Hermitian systems, Rev. Mod. Phys. **93**, 015005 (2021).

[81] H. Weimer, A. Kshetrimayum, and R. Orús, Simulation methods for open quantum many-body systems, Rev. Mod. Phys. **93**, 015008 (2021).

[82] M. Esposito, U. Harbola, and S. Mukamel, Nonequi-

librium fluctuations, fluctuation theorems, and counting statistics in quantum systems, Rev. Mod. Phys. **81**, 1665 (2009).

[83] F. Verstraete, M. M. Wolf, and J. Ignacio Cirac, Quantum computation and quantum-state engineering driven by dissipation, Nat. Phys. **5**, 633 (2009).

[84] T. Prosen and I. Pižorn, Quantum phase transition in a far-from-equilibrium steady state of an XY spin chain, Phys. Rev. Lett. **101**, 105701 (2008).

[85] H. T. Mebrahtu, I. V. Borzenets, H. Zheng, Y. V. Bomze, A. I. Smirnov, S. Florens, H. U. Baranger, and G. Finkelstein, Observation of Majorana quantum critical behaviour in a resonant level coupled to a dissipative environment, Nat. Phys. **9**, 732 (2013); H. T. Mebrahtu, I. V. Borzenets, D. E. Liu, H. Zheng, Y. V. Bomze, A. I. Smirnov, H. U. Baranger, and G. Finkelstein, Quantum phase transition in a resonant level coupled to interacting leads, Nature (London) **488**, 61 (2012).

[86] M. V. Medvedyeva, M. T. Čubrović, and S. Kehrein, Dissipation-induced first-order decoherence phase transition in a noninteracting fermionic system, Phys. Rev. B **91**, 205416 (2015).

[87] K. Shastri and F. Monticone, Dissipation-induced topological transitions in continuous Weyl materials, Phys. Rev. Res. **2**, 033065 (2020).

[88] A. M. Lacerda, J. Goold, and G. T. Landi, Dephasing enhanced transport in boundary-driven quasiperiodic chains, Phys. Rev. B **104**, 174203 (2021).

[89] D. Dwiputra and F. P. Zen, Environment-assisted quantum transport and mobility edges, Phys. Rev. A **104**, 022205 (2021).

[90] M. Soriente, T. L. Heugel, K. Arimitsu, R. Chitra, and O. Zilberberg, Distinctive class of dissipation-induced phase transitions and their universal characteristics, Phys. Rev. Res. **3**, 023100 (2021).

[91] W. Nie, M. Antezza, Y.-X. Liu, and F. Nori, Dissipative topological phase transition with strong system-environment coupling, Phys. Rev. Lett. **127**, 250402 (2021).

[92] K. Yamamoto, M. Nakagawa, N. Tsuji, M. Ueda, and N. Kawakami, Collective excitations and nonequilibrium phase transition in dissipative fermionic superfluids, Phys. Rev. Lett. **127**, 055301 (2021).

[93] K. Kawabata, T. Numasawa, and S. Ryu, Entanglement Phase Transition Induced by the Non-Hermitian Skin Effect, Phys. Rev. X **13**, 021007 (2023).

[94] E. I. R. Chiacchio, A. Nunnenkamp, and M. Brunelli, Nonreciprocal Dicke Model, Phys. Rev. Lett. **131**, 113602 (2023).

[95] Y. Liu, Z. Wang, C. Yang, J. Jie, and Y. Wang, Dissipation-induced extended-localized transition, Phys. Rev. Lett. **132**, 216301 (2024).

[96] S. Longhi, Dephasing-induced mobility edges in quasicrystals, Phys. Rev. Lett. **132**, 236301 (2024).

[97] G. Lindblad, On the generators of quantum dynamical semigroups, Commun. Math. Phys. **48**, 119 (1976).

[98] H.-P. Breuer and F. Petruccione, *The Theory of Open Quantum Systems* (Oxford University Press, Oxford, 2002).

[99] B. Kraus, H. P. Büchler, S. Diehl, A. Kantian, A. Micheli, and P. Zoller, Preparation of entangled states by quantum Markov processes, Phys. Rev. A **78**, 042307 (2008).

[100] C.-E. Bardyn, M. A. Baranov, C. V. Kraus, E. Rico, A. Imamoğlu, P. Zoller, S. Diehl, Topology by dissipation, New J. Phys. **15**, 085001 (2013).

[101] D. Marcos, A. Tomadin, S. Diehl, and P. Rabl, Photon condensation in circuit quantum electrodynamics by engineered dissipation, New J. Phys. **14**, 055005 (2012).

[102] I. Yusipov, T. Laptyeva, S. Denisov, and M. Ivanchenko, Localization in open quantum systems, Phys. Rev. Lett. **118**, 070402 (2017); O. S. Vershinina, I. I. Yusipov, S. Denisov, M. V. Ivanchenko, and T. V. Laptyeva, Control of a single-particle localization in open quantum systems, Europhys. Lett. **119**, 56001 (2017); I. I. Yusipov, T. V. Laptyeva, and M. V. Ivanchenko, Quantum jumps on Anderson attractors, Phys. Rev. B **97**, 020301 (2018); I. Vakulchyk, I. Yusipov, M. Ivanchenko, S. Flach, and S. Denisov, Signatures of many-body localization in steady states of open quantum systems, Phys. Rev. B **98**, 020202(R) (2018).

[103] Y. Peng, C. Yang, and Y. Wang, Manipulating the relaxation time of boundary-dissipative systems through bond dissipation, Phys. Rev. B **110**, 104305 (2024); Y. Hu, C. Yang, and Y. Wang, Inducing a transition between thermal and many-body localized states and detecting many-body mobility edges through dissipation, arXiv:2407.13655; X. Yang, X.-P. Jiang, Z. Wei, Y. Wang, and L. Pan, arXiv:2409.20319; Y. Peng, C. Yang, H. Hu, and Y. Wang, Dissipation-assisted preparation of topological boundary states, arXiv:2412.04152.

[104] See the Supplemental Material for details on the physical effects of different bond dissipation configurations between the upper and lower chains.

Supplementary Material:
Dissipation-Driven Transition of Particles from Dispersive to Flat Bands

In the main text, we require identical forms of bond dissipation for both the upper and lower chains, i.e., $Q_j^u = Q_j^l$, while allowing the dissipation strengths Γ of the two chains to differ. In the Supplementary Materials, we examine the physical consequences arising from distinct bond dissipation configurations between the upper and lower chains. We fix the dissipation strength Γ on both chains to be 1. We denote the elements in the bond dissipation operator O^u applied to the upper chain as a^u and q^u, and those in the bond dissipation operator O^l applied to the lower chain as a^l and q^l.

I. $a^u \neq a^l$

We take the cross-stitch model as an example, keeping q of both the upper and lower chains fixed at 1. However, the bond dissipation added to the upper chain is set to $a = 1$, while the bond dissipation added to the lower chain is set to $a = -1$. Fig.S1 demonstrates that the system's steady state does not exclusively occupy the flat band (FB) region. This can be understood as follows: While different compact localized states (CLSs) may acquire arbitrary relative phases, the intra-CLS phase difference between upper and lower chains is fixed. For instance, the CLS in the cross-stitch model takes the form $|\phi_{\mathrm{CLS}}\rangle = (1, -1)^T$, indicating opposite phases on the two chains. The condition $a^u = 1$ requires identical phases between neighboring sites on the upper chain for steady-state formation. If the steady state were composed of CLS superpositions, this would further impose identical phases between lower-chain neighbors (as all lower-chain occupations must maintain π-phase opposition to the upper chain). However, $a^l = -1$ favors anti-phase configurations between neighboring sites, thereby disrupting the CLS construction. Consequently, the asymmetry condition $a^u \neq a^l$ prevents complete FB occupation in the final steady state.
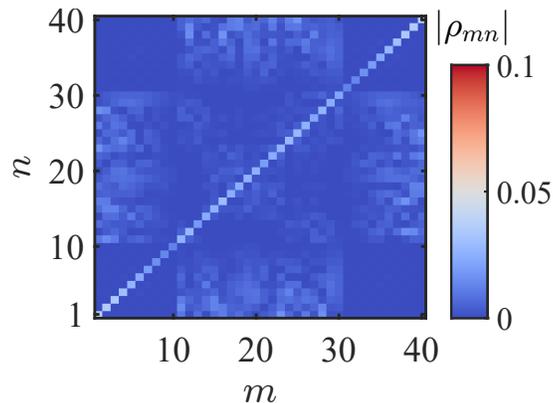

Figure S1: The absolute values of the steady state's density matrix elements in the eigenbasis of H. We employ identical conditions and parameters as in Fig. 2 of the main text, except for modifying the previously equal chain coefficients to asymmetric values $a^u = 1$ and $a^l = -1$.

II. $q^u \neq q^l$

We take the sawtooth model as an example, keeping a of both the upper and lower chains fixed at 1. However, q^u and q^l are different, with $q^u = 1$ and $q^l = 2$. Fig. S2(a)(b) and Fig. 4(a)(c) in the main text are exactly the same. This system's steady state is occupied in the FB region and is a pure state, which also exhibits an in-phase distribution between next-nearest-neighbor lattice sites on the lower chain, while on the upper chain, neighboring lattice sites share the same phase distribution. Such a choice of bond dissipation depends on the configuration of the CLS in the sawtooth lattice. Each CLS occupies two unit cells, where the distribution within a CLS is such that neighboring lattice sites on the upper chain have the same phase (thus, when $q^u = 1$, only $a = 1$ is allowed, and $a = -1$ is not allowed), while on the lower chain, one site is occupied while the other remains unoccupied (see Fig.1(c) in the main text). Therefore, when the specific configuration of the CLS is known in advance, the form of

bond dissipation can be designed based on the characteristics of the CLS, and it does not necessarily need to satisfy Eq. (5) in the main text. However, Eq. (5) in the main text is always capable of achieving a steady-state occupation in the FB, regardless of the model or the form of the CLS.
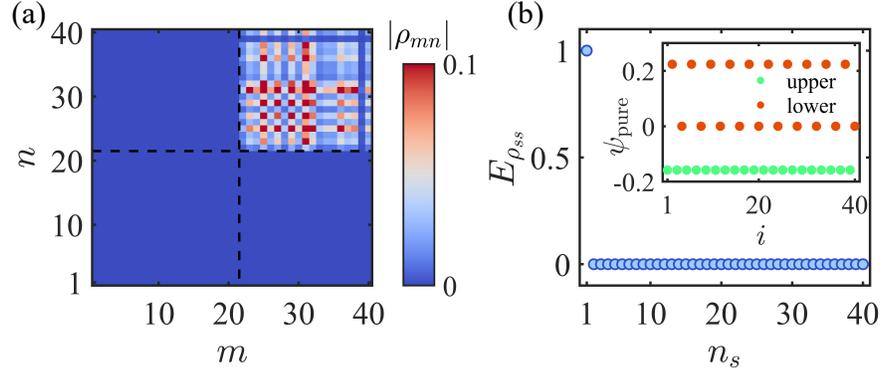

Figure S2: We adopt the same conditions and parameters as those in Fig. 4(a) of the main text, except that we modify the originally equal chain coefficients from $q^u = q^l = 2$ to $q^u = 1$ and $q^l = 2$. Note that in this case, we fix $a = 1$. $a = -1$ cannot achieve a steady-state occupation in the FB.